The inhibitory effect of certain imidazole derivatives grafted on 8-hydroxyqinoline on carbon steel corrosion in acidic medium: experimental and computational approaches

A. Elbarki,[1] Z. Amrani,[2] T. Laabaissi,[1] M. El Faydy,[3] L. Adlani,[1] A. Fatah,[1] F. Benhiba,[2,4] M. Rbaa,[3] I. Warad,[5] B. Lakhrissi,[3] H. Zarrok,[1] A. Bellaouchou,[2] B. Dikici,[6] H. Oudda[1] and A. Zarrouk[2]*

[1]Laboratory of Separation Processes, Department of Chemistry, Faculty of Sciences, Ibn Tofaïl University, PO Box 133, 14000 Kenitra, Morocco
[2]Laboratory of Materials, Nanotechnology and Environment, Faculty of Sciences, Mohammed V University in Rabat, Av. Ibn Battouta, P.O. Box 1014 Agdal-Rabat, Morocco
[3]Laboratory of Organic Chemistry, Inorganic, Electrochemistry, and Environment, Department of Chemistry, Faculty of Sciences, Ibn Tofaïl University, PO Box 133, 14000 Kenitra, Morocco
[4]Higher Institute of Nursing Professions and Health Techniques of Agadir, Annex Guelmim, Morocco
[5]Department of Chemistry, AN-Najah National University, P.O. Box 7, Nablus, Palestine
[6]Laboratory of Corrosion, Department of Metallurgical and Materials Engineering, Ataturk University, 25240 Erzurum, Turkey

**E-mail: azarrouk@gmail.com*

Abstract

In this work, we scrutinized two imidazole derivatives grafted on 8-hydroxyqinoline, namely 5-((2-(4-hydroxyphenyl)-4,5-diphenyl-1*H*-imidazol-1-yl)methyl)quinolin-8-ol (HDIQ) and 5-((2-([1,1′-diphenyl]-4-yl)-4,5-diphenyl-1*H*-imidazol-1-yl)methyl)quinolin-8-ol (BDIQ), as corrosion inhibitors for carbon steel (CS) in HCl environment. Evaluation of their inhibitory properties was carried out using weight loss (WL) and electrochemical techniques such as potentiodynamic polarization curves (PDP) and electrochemical impedance spectroscopy (EIS). In addition, the metal surface was characterized by surface morphology analysis using a scanning electron microscope (SEM) and energy-dispersive X-ray spectroscopy (EDS). The inhibitory efficiencies of HDIQ and BDIQ increase with concentration, reaching a maximum inhibitory efficiency of 90.8% for HDIQ and 87.5% for BDIQ at 10^{-3} M. Temperature effects on inhibitory efficiency were investigated in the [303–333 K] range. The adsorption of BDIQ and HDIQ onto the CS surface in the corrosive environment followed the Langmuir isotherm. Morphological SEM images provide satisfactory confirmation of the results obtained during WL and electrochemical tests. Quantum theoretical studies using density functional theory (DFT) and molecular dynamics (MD) simulations confirmed the experimental results.

Received: August 31, 2023. Published September 12, 2023 doi: 10.17675/2305-6894-2023-12-3-27

Keywords: *corrosion inhibition, carbon steel, 8-hydroxyquinoline-imidazole, EDS/SEM, DFT/MD.*

1. Introduction

Studying the corrosion of CS in an acidic environment is of considerable importance due to the increasing use of CS in various industrial sectors [1]. Hydrochloric acid finds widespread application in acid pickling, scale removal, and cleaning processes, as well as in the acidification of metal oil wells. Nevertheless, its corrosive ions can cause damage to metal surfaces [2]. One of the most effective approaches to corrosion prevention is the use of organic corrosion inhibitors. These agents bind to metal surfaces, creating a thin protective layer that insulates the metal from aggressive ions present in the corrosive environment [3]. This technique is characterized by its remarkable effectiveness in inhibiting corrosion while offering the advantages of moderate cost, low toxicity, and high efficiency [4]. Heterocyclic structures with aromatic rings and polar groups act as brilliant corrosion inhibitors [5–10]. These compounds are more able to bond to metal surfaces and form a barrier that shields them from corrosion because they contain heteroatoms and polar functional groups [11]. The physical and chemical characteristics of the inhibitor molecule as well as the metal surface and the electrolyte medium, as well as other variables, determine the interactions between the inhibitor molecule and the metal surface [12].

Quinolines are particularly noteworthy in this regard among the many organic corrosion inhibitors that have been created to protect iron and its alloys in acidic environments [13]. Research has indicated that different variations of 8-hydroxyquinoline have proven to be highly effective corrosion inhibitors in extremely corrosive surroundings [14–18]. The metals on which these studies have focused include various steels (CS, mild steel, *etc.*), as well as pure metals such as zinc, aluminum, iron, copper, and their alloys. The exploration of new 8-hydroxyquinoline derivatives continues to grow significantly due to their potential applications in various fields, particularly biology and medicinal chemistry [19, 20]. Attaching this 8-hydroxyquinoline to another group, such as imidazole, leads to an increase in efficiency and an improvement in its corrosion resistance at very low concentrations and high temperatures. It is in this context that our present work will be done.

In this study, the objective is to establish a correlation between the molecular structure of two imidazole derivatives grafted on 8-hydroxyqinoline and their effectiveness in inhibiting corrosion for CS in the acidic medium. The inhibitory performance of the compounds was evaluated using the WL, PDP, and EIS. The metal surface was characterized by surface morphology analysis (EDS and SEM). The inhibition potential was also elucidated by quantum calculations to facilitate the interpretation of its effectiveness. The adsorption mechanisms of HDIQ and BDIQ on the CS surface were also explained by use of global quantum chemical descriptors and MD simulations.

2. Experimental procedure

2.1. Materials, specimen, medium, and inhibitor

In proportion to weight, CS has the following elements: 0.370% C, 0.680% Mn, 0.059% Ni, 0.009% Co, 0.160% Cu, 0.016% S, 0.011% Ti, 0.230% Si, 0.077% Cr, and the rest fraction of iron (Fe). 1 M HCl hydrochloric acid was made by diluting 37% AR-grade hydrochloric acid with distilled water. Table 1 displays the molecular nomenclature, structure, and abbreviations of the 8-hydroxyquinoline-imidazole derivatives under examination.

Table 1. Structures and nomenclatures of 8-Hydroxyquinoline-imidazole derivatives.

Structures	Abbreviation	Nomenclatures
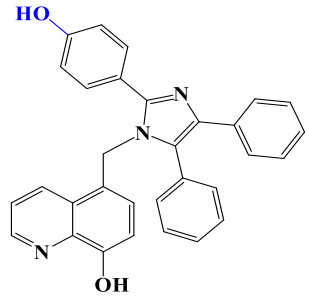	HDIQ	5-((2-(4-hydroxyphenyl)-4,5-diphenyl-1*H*-imidazol-1-yl)methyl)quinolin-8-ol
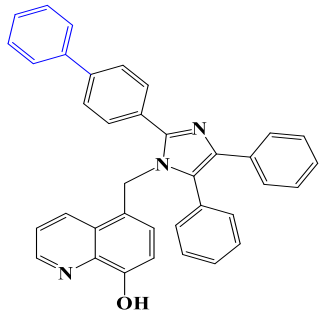	BDIQ	5-((2-([1,1′-biphenyl]-4-yl)-4,5-diphenyl-1*H*-imidazol-1-yl)methyl)quinolin-8-ol

2.2. WL study

The WL tests were executed in accordance with ASTM [21]. The rectangular-shaped CS samples, measuring 1 cm×2 cm×0.1 cm, with and without BDIQ and HDIQ, were dipped in 1 M HCl for 6 hours at 303 K. The following equations (1) and (2) [22] establish the corrosion rate (W) and inhibition efficiency (E_w (%)) for BDIQ and HDIQ:

$$W = \frac{\Delta m}{S \times t} \tag{1}$$

$$E_w(\%) = \frac{W - W_{inh}}{W} \times 100 \tag{2}$$

where Δm refers to the mass loss, S refers to the CS surface, t refers to the dipping time, W and W_{inh} refer to the corrosion rate in the absence and presence of BDIQ and HDIQ, respectively.

2.3. PDP and EIS tests

Using the potentiostat model PGZ 100 associated with Volta-Master 4 software equipment, electrochemical research was carried out in a three-electrode cell. Platinum (Pt) was used as the counter electrode, a saturated calomel electrode was chosen as the reference electrode (SCE), and CS with an area of 1 cm^2 was chosen as the working electrode. Before each electrochemical experiment, the CS was immersed in 50 mL of 1 M HCl for half an hour to achieve a steady OCP and equilibrium potential.

The EIS experiment was conducted at OCP in the frequency range of 100 kHz to 10 mHz, with a signal amplitude of 10 mV. The inhibitory action (η_{EIS} (%)) was determined as [22]:

$$\eta_{EIS}(\%) = \left(\frac{R_{P,i} - R_{P,0}}{R_{P,i}} \right) \times 100 \quad (3)$$

where $R_{P,i}$ and $R_{P,0}$ are defined as the polarization resistance with and without BDIQ and HDIQ, respectively.

PDP plots were recorded by changing the electrode potential automatically from (–0.8 to –0.1 V) *versus* SCE with a scan rate of 0.5 mV s^{-1}. The inhibitory action (η_{PDP} (%)) was defined as [22]:

$$\eta_{PDP}(\%) = \left(\frac{i_{corr,0} - i_{corr}}{i_{corr,0}} \right) \times 100 \quad (4)$$

where $i_{corr,0}$ and i_{corr} was defined as the corrosion current density without and with BDIQ and HDIQ, respectively.

In the absence of BDIQ and HDIQ, we used the previously published results from our team for both the stationary and transitory techniques regarding the effect of the temperature and concentration. These experiments were conducted under similar circumstances [23, 24].

2.4. Surface investigation

The surface morphologies of the specimens, which were exposed to the acidic medium with and without 10^{-3} M BDIQ and HDIQ for 24 h at 303 K, were analyzed using the (JEOL-JSM-IT-100, JEOL, Akishima, Tokyo) was used to analyze the surface morphology and energy-dispersive X-Ray spectroscopy (EDS) (Thermo Fisher, Waltham, MA, USA). We used the results of the blank in the absence and presence of HCl without inhibitors, since we worked under similar conditions in a work submitted simultaneously with this one [25].

2.5. Theoretical details

In the current study, the ground-state geometries for the HDIQ and BDIQ were performed by using DFT in conjunction with Becke's [26, 27] three-parameter exchange functional along with the Lee-Yang-Parr [21] nonlocal correlation functional (B3LYP) and 6-311++G

(d, p) basis set. A polarizable continuum model of solvation (PCM) was employed for the aqueous solution. The most important key information that can be obtained from the optimized structures is the frontier molecular orbitals (FMO) (highest occupied molecular orbitals (HOMO) and lowest unoccupied molecular orbitals (LUMO)) and energy gaps (ΔE).

To confirm that the optimized geometries are local minima on the potential energy surfaces, we have carried out frequency calculations using the same level of theory. The Gaussian 09 program package was used to carry out all calculations [28].

The global chemical reactivity descriptors E_{HOMO}, E_{LUMO}, ΔE, absolute electronegativity (χ), chemical hardness (η), and the fraction of electrons transferred (ΔN_{110}) were calculated using the following equations [29]:

$$\chi = \frac{1}{2}\left(E_{HOMO} + E_{LUMO}\right) \tag{5}$$

$$\eta = \frac{1}{2}\left(E_{HOMO} - E_{LUMO}\right) \tag{6}$$

$$\Delta N_{110} = \frac{\chi_{Fe_{110}} - \chi_{inh}}{2\left(\eta_{Fe_{110}} + \eta_{inh}\right)} = \frac{\Phi_{Fe} - \chi_{inh}}{2\eta_{inh}} \tag{7}$$

Here, the work function of the Fe (110) plane (Φ_{Fe}) was taken to be 4.82 eV, the hardness of Fe, $\eta_{Fe_{110}}$ =0 eV was taken, and the assumption that for a bulk metal I=A because they are softer than the neutral metallic atoms [27]. ΔN_{110}<3.6 signifies that the inhibitor can be used in the direction of electron transfer during the adsorption process [30].

2.6. Molecular dynamics (MD) simulation

MD simulations, in particular, allow for the establishment of the degree of interaction between the examined species and the Fe (110) structures. Similar to our prior work [31], we utilized the forcite module included with the Materials Studio/8 program to do this simulation with a simulation box (27.30×27.30×37.13 Å^3). This vacuum has 491 H_2O, 9 H_3O^+, 9 Cl^-, and inhibitors in it. Under the COMPASS force field, the Andersen thermostat sets the temperature of the modeled environment to 303 K for the NVT ensemble for simulation times of “1000 ps” and “1 fs” [32].

3. Results and Discussion

3.1. WL measurements

The W and E_w (%) values of various concentrations for HDIQ and BDIQ in 1M HCl at 303 K were calculated and summarized in Table 2. From this table it is clear that inclusion of HDIQ and BDIQ molecules into the corrosive medium reduces W and improves E_w (%). This may be due to the HDIQ and BDIQ binding to the CS *via* lone pairs of nitrogen and oxygen atoms

as well as the electrons of the quinoline and imidazole rings, which results in coating the metal surface and forming a protective film [33]. However, among the concentrations evaluated, HDIQ and BDIQ at 10^{-3} M manifest the best inhibitory effectiveness reaching 95.6% and 93.5%, respectively. Furthermore, HDIQ outperforms BDIQ in terms of inhibiting performance, which may be attributed to its effect on the hydroxyl group (–OH) in HDIQ rather than the phenyl group ($-C_6H_5$) in BDIQ. By the mesomeric effect, the hydroxyl group acts as a donor, contributing to an enhancement of the electron density at the adsorption sites of the HDIQ molecule and so boosting adsorption capability. In addition, the BDIQ and HDIQ molecules can easily be protonated to form cation-ionic forms in HCl solution and therefore adsorb at the metal surface through the already adsorbed chloride ions. Also, the adsorption of the neutral BDIQ and HDIQ molecules could occur through the formation of links between the d-orbital of iron atoms, involving the displacement of water molecules from the metal surface, and the lone sp^2 electron pairs present on the N, O atoms and π-orbitals in the aromatic ring, blocking the active sites on the steel surface and therefore decreasing the corrosion rate.

Table 2. *W* and E_w(%) for CS corrosion in the inhibited medium and its non-inhibited counterpart.

Medium	***C* (M)**	***W* (mg/cm^2·h^{-1})**	**E_w (%)**
1 M HCl	00	2.341	–
BDIQ	10^{-3}	0.151	93.5
	10^{-4}	0.293	87.4
	10^{-5}	0.603	74.2
	10^{-6}	0.693	70.3
HDIQ	10^{-3}	0.101	95.6
	10^{-4}	0.221	90.5
	10^{-5}	0.529	77.4
	10^{-6}	0.587	74.9

3.2. Electrochemical study

3.2.1. PDP plots

The polarization curves for CS in 1 M HCl at 303 K are shown in Figure 1, both in the presence of BDIQ and HDIQ and when they are absent, at concentrations ranging from 10^{-3} to 10^{-6} M. The electrochemical parameters derived from these curves are presented in Table 3. The parallel cathodic Tafel curves revealed that hydrogen evolution was activation controlled and that the presence of the inhibitors had no influence on the reduction process [34, 35]. A closer look at Figure 2 shows that the values of i_{corr} for CS in the presence of HDIQ and BDIQ were lower than those for the non-inhibited solution. Anodic and cathodic currents both decreased. This result suggests that the Cl^- attack on the CS was hindered by

the interaction of HDIQ and BDIQ. Inhibition of both the hydrogen evolution and CS dissolving processes is indicated by the decrease in corrosion rate with increased HDIQ and BDIQ concentrations, as well as a change in both the cathodic and anodic Tafel branches of the polarization curves to lower current density values [25]. It is worth noting that the HDIQ and BDIQ decrease the current densities, and their effect becomes more efficient when the HDIQ and BDIQ concentration increases, indicating the formation of a protective layer reducing, therefore, the corrosion rate and blocking the anodic and cathodic sites.

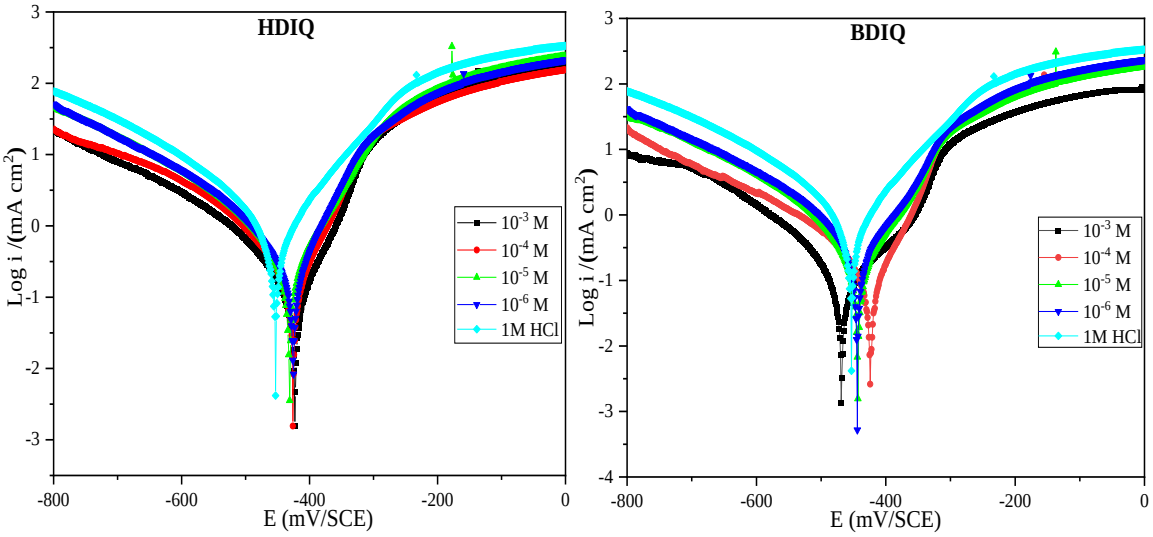

Figure 1. PDP charts for CS corrosion in the inhibited medium and its non-inhibited counterpart.

Miscellaneous PDP indices like cathodic (β_c), anodic Tafel slopes (β_a), and corrosion potential (E_{corr}) were acquired from the PDP curve extrapolation (Table 3). The difference in E_{corr} between inhibited and non-inhibited mediums does not surpass 63.5 mV/SCE, indicating the mixed-type character of both HDIQ and BDIQ [36]. Furthermore, the findings in Table 3 reveal more dramatic variations in the values of β_c and β_a, indicating the mixed behavior of both HDIQ and BDIQ [37]. The β_c values, also, change when BDIQ and/or HDIQ are added, indicating a modification of the mechanism of hydrogen evolution. This implies that BDIQ and HDIQ successfully block the corrosion process of CS, and their effectiveness as corrosion inhibitors grows as their concentration is raised. The monolayer formed on the surface as a result of the adsorbed quinoline molecules may be the cause of the inhibition of the cathodic process [18]. However, it is clear that when BDIQ and/or HDIQ are present, the value of β_a significantly changes from the blank case, indicating that BDIQ and/or HDIQ may have an impact on the anodic process' kinetics. According to the BDIQ and/or HDIQ structures, the atoms of nitrogen and oxygen in the quinolinol rings have a number of lone pairs of electrons. This might alter the iron's dissolving process by encouraging the production of the complex molecules Fe(II)–BDIQ and Fe(II)–HDIQ [23, 24]. Furthermore, the η_{PDP} (%) values improve with concentration, reaching 92.8% for HDIQ and 89.3% for BDIQ at 0.001 M, respectively. The improvement in η_{PDP} (%) with concentration may be owing to the formation of the protector film, which prevents

the acid medium from attacking the metal surface due to the adsorption of adsorbed species of HDIQ and BDIQ on the CS surface as a result of the interactions between the π-electrons and heteroatoms of quinoline and imidazole rings and the vacant *d*-orbitals of Fe atoms.

Table 3. PDP indices for CS corrosion in the inhibited medium and its non-inhibited counterpart.

Medium	*C* (M)	$-E_{corr}$ (mV/SCE)	i_{corr} (μA·cm^{-2})	$-\beta_c$ (mV·dec^{-1})	β_a (mV·dec^{-1})	η_{PDP} (%)
1 M HCl	00	456.3	1104.1	112.8	155.4	–
BDIQ	10^{-6}	394.2	742.8	149.3	50.5	32.7
	10^{-5}	430.1	413.0	117.2	73.6	62.5
	10^{-4}	423.9	286.6	132.4	68.0	74.4
	10^{-3}	425.3	118.3	111.0	64.3	89.3
HDIQ	10^{-6}	468.0	317.9	131.6	90.2	71.2
	10^{-5}	443.4	275.4	128.9	85.2	75.0
	10^{-4}	424.4	160.2	142.8	66.9	85.5
	10^{-3}	468.2	79.1	86.0	76.5	92.8

3.2.2. EIS plots

The EIS approach may offer detailed data on the kinetics of electrode processes in addition to the characteristics of the CS surface. The Nyquist charts of CS in non-inhibited and inhibited mediums are shown in Figure 2. In the non-inhibited medium, a somewhat depressed capacitive loop was viewed for CS (Figure 2). Also, the addition of HDIQ and/or BDIQ had no effect on the profile of the depressed semicircular Nyquist plots. This trend implies that CS corrosion is mostly charge-transfer-based, with no changes in the process of the corrosion reaction [38]. Inhomogeneity as well as other types of interfacial phenomena in both non-inhibited and inhibited media may contribute to the departure from the ideal semi-circular shape, known as the frequency dispersion of the interfacial impedance [39]. Besides, the semicircle size augmented upon the introduction of HDIQ and BDIQ meaning that 8-hydroxyquinoline imidazole derivatives self-assemble on the CS interface to produce a protective layer. Table 4 provides the EIS indices collected by fitting the Nyquist charts with the basic equivalent circuit (EC), as depicted in Figure 3. A medium resistance (R_m) and a constant phase element (*CPE*) parallel to the polarization resistance (R_p) were incorporated in the applied EC. To reduce fluctuations brought on by frequency dispersion, *CPE* was utilized inside the EC in place of the optimum capacitance capacity of a double layer (C_{dl}) [40]. The impedance of CPE (Z_{CPE}) and C_{dl} can be related by the next expression [41, 42]:

$$Z_{CPE} = \left(\frac{1}{Q \times (i \times w)^n} \right) \quad (8)$$

$$C_{\mathrm{dl}} = \left(Q \times \left(R_{\mathrm{p}}\right)^{1-n}\right)^{1/n} \tag{9}$$

where Q denotes the CPE magnitude; i stands for the imaginary root; w stands for the angular frequency; n denotes the deviation index ($-1 \leq n \leq 1$) that quantifies the deviation from ideal capacitive conduct.

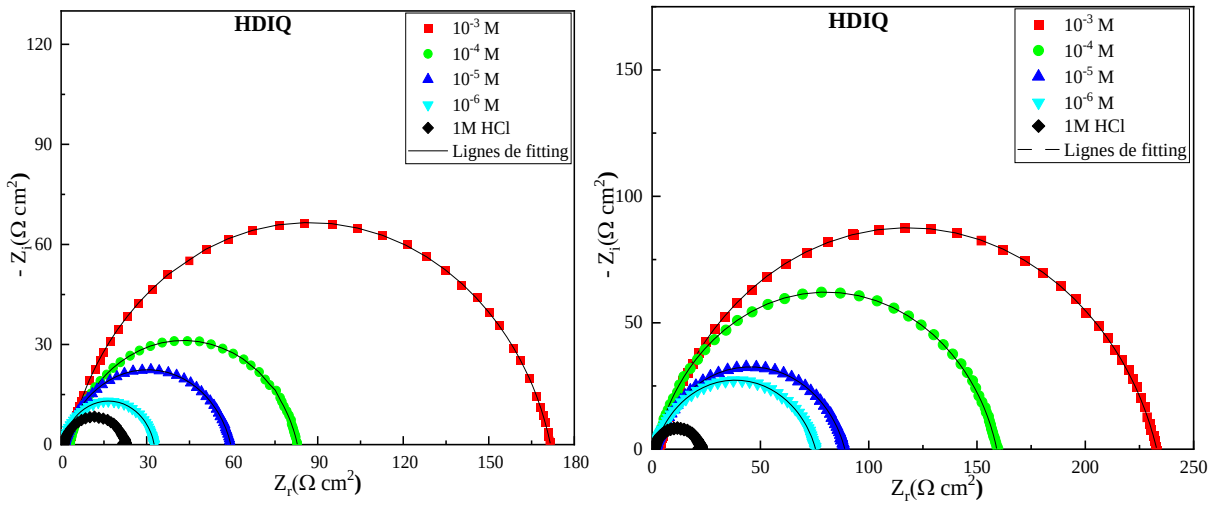

Figure 2. Nyquist charts for CS corrosion in the inhibited medium and its non-inhibited counterpart.

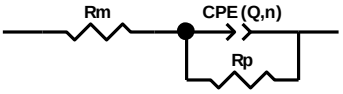

Figure 3. The proposed EC to fit Nyquist plots.

Table 4. EIS indices for CS corrosion in the inhibited medium and its non-inhibited counterpart.

Medium	***C* (M)**	R_{m} **(Ω·cm²)**	R_{p} **(Ω·cm²)**	C_{dl} **(μF·cm⁻²)**	***n***	***Q*** **(μF·s^{n-1}·cm⁻²)**	η_{EIS} **(%)**	**θ**
1 M HCl	00	0.83	21.57	116.2	0.845	293.9	–	–
BDIQ	10^{-6}	0.60	32.02	97.4	0.830	205.0	32.8	0.328
	10^{-5}	1.19	58.29	82.2	0.836	197.4	63.1	0.631
	10^{-4}	2.99	79.87	71.0	0.840	158.2	73.1	0.731
	10^{-3}	2.70	168.9	80.9	0.850	153.8	87.2	0.872
HDIQ	10^{-6}	1.27	74.20	92.4	0.840	250.3	71.0	0.710
	10^{-5}	1.27	87.40	65.7	0.842	180.6	75.0	0.750
	10^{-4}	1.49	154.9	63.5	0.848	128.2	86.2	0.862
	10^{-3}	2.93	221.3	46.6	0.850	92.60	90.2	0.902

As evident from Table 4, the R_p values augment with an increase in the concentration of the BDIQ and HDIQ, while the C_{dl} values exhibit the opposite trend. This can be attributed to an upsurge in surface coverage on the CS surface due to BDIQ and HDIQ adsorption. The reduction in Q and C_{dl} is associated with the increase in double-layer thickness owing to the substitution of water molecules at the CS/medium interface by the BDIQ and HDIQ molecules through the adsorption process [43, 44]. The values of n for BDIQ and HDIQ are larger than those in the non-inhibited medium, indicating that the adsorption of these derivatives has resulted in a smoother CS surface [45]. These findings demonstrate that BDIQ and HDIQ shield the carbon steel surface from corrosion in 1 M HCl medium by producing a protective barrier, and the sequence of η_{EIS} (%) is HDIQ > BDIQ. These findings are comparable with those obtained using PDP and WL [46].

3.3. Adsorption isotherm

Adsorption isotherms offer substantial details regarding the inhibitorɔs adsorption on the metal surface. Multiple isotherm models, including Langmuir, Frumkin, and Temkin isotherms, were applied to fit the experimental findings [47]. To calculate the surface coverage (θ) it was assumed that the inhibitor efficiency is due mainly to the blocking effect of the adsorbed species:

(Langmuir) $$C/\theta = 1/K_{ads} + C \quad (10)$$

(Frimkin) $$\left(\frac{\theta}{1-\theta}\right)\exp(2b\theta) = K_{ads}C \quad (11)$$

(Temkin) $$\exp(-2b\theta) = K_{ads}C \quad (12)$$

where θ denotes the surface coverage which is equal to η_{EIS}(%)/100, b denotes the constant of molecular interaction, and K_{ads} denotes the equilibrium constant.

The Langmuir adsorption isotherm appears to offer the most accurate representation of the adsorption process of the examined BDIQ and HDIQ in this work, with R^2 and slope values near 1 (Figure 4).

The free energy of adsorption (ΔG_{ads}) and the K_{ads} can be expressed as follow [48]:

$$\ln K_{ads} = -\frac{\Delta G_{ads}}{RT} - \ln(55.5) \quad (13)$$

The values of adsorptive indices are summarized in Table 5. The strong connection between the adsorbed molecules and the metal surface is evidenced by the high K_{ads}(BDIQ) > K_{ads}(HDIQ) values, suggesting that the 8-hydroxyquinoline molecules are strongly bonded and cannot be easily released by acidic molecules [49]. The K_{ads}(HDIQ) > K_{ads}(BDIQ) imply that HDIQ performed more efficiently than BDIQ. Furthermore, adsorption is classified as chemical, physical, or both based on ΔG_{ads} levels. According to previous research, ΔG_{ads} levels close to −40 kJ/mol or more negative are associated with chemical adsorption, while those close to −20 kJ/mol or more positive are

related to physical adsorption [24]. The respective ΔG_{ads} values for BDIQ and HDIQ are negative than –40 kJ/mol, implying that BDIQ and HDIQ adsorption involve chemisorption.

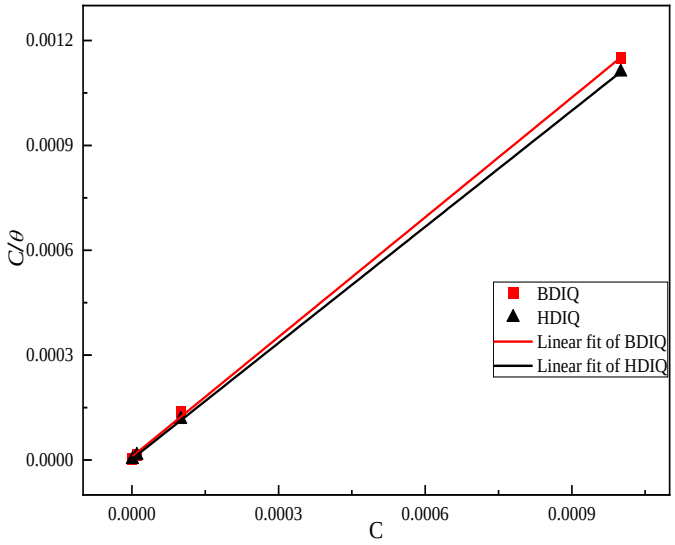

Figure 4. Langmuir adsorption isotherm for CS corrosion in the presence of BDIQ and HDIQ in 1 M HCl at 303 K.

Table 5. Adsorption indices for HDIQ and BDIQ.

	R^2	Slope	K_{ads} (L/mol)	ΔG_{ads} (kJ·mol^{-1})
HDIQ	0.999	1.106	3.91×10^5	–42.53
BDIQ	0.999	1.138	1.07×10^5	–39.27

3.4. Temperature effect and activation indices

The implications of temperature on CS dissolution in the acidic medium blank and with 10^{-3} M of HDIQ or BDIQ have been assessed through PDP recordings at temperatures that stretch from 303 to 333 K, as displayed in Figure 5. Table 6 provides their relevant electrochemical indices. Clearly, i_{corr} elevates with elevated temperatures in both the non-inhibited and inhibited mediums, while the η_{PDP} (%) of HDIQ and BDIQ diminish. As a result, the η_{PDP} (%) of HDIQ and BDIQ were considerably temperature-dependent. This conduct can be accounted for by the fact that temperature alters the adsorption-desorption equilibria favoring the desorption of 8-hydroxyquinoline derivatives from CS [50]. While HDIQ continues to outperform BDIQ.

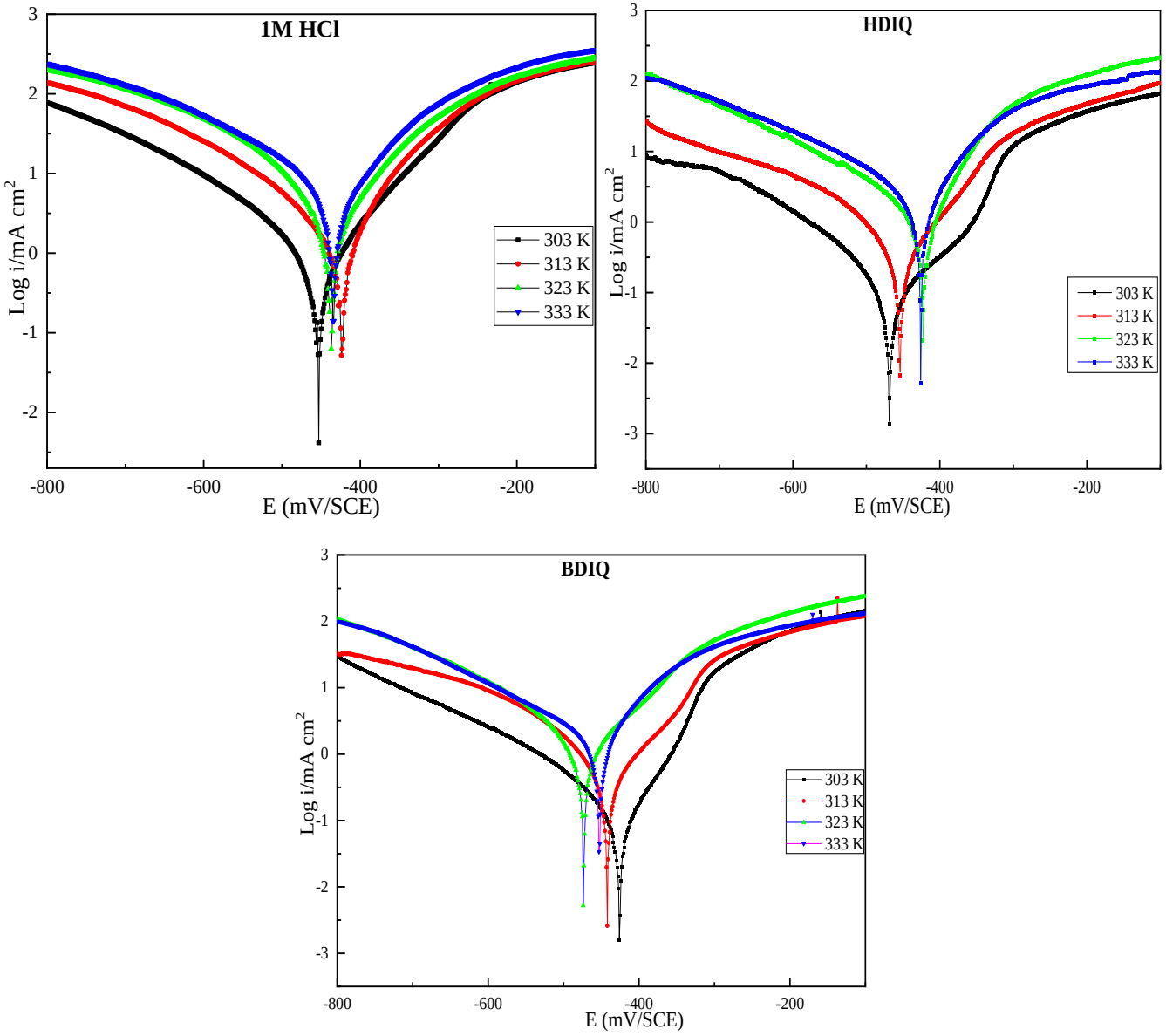

Figure 5. PDP charts for CS dissolution in the inhibited medium and its non-inhibited counterpart at divers' temperatures.

Table 6. PDP indices for CS dissolution in the inhibited medium and its non-inhibited counterpart at divers' temperatures.

Medium	T (K)	$-E_{corr}$ (mV/SCE)	i_{corr} (μA·cm^{-2})	$-\beta_c$ (mV·dec^{-1})	β_a (mV·dec^{-1})	η_{PDP} (%)
1 M HCl	303	456.3	1104	112	155.4	–
	313	423.5	1477.4	131.3	91.3	–
	323	436.3	2254	117.8	91.4	–
	333	433.3	3944.9	134.6	103.9	–

Medium	T (K)	$-E_{corr}$ (mV/SCE)	i_{corr} ($\mu A \cdot cm^{-2}$)	$-\beta_c$ ($mV \cdot dec^{-1}$)	β_a ($mV \cdot dec^{-1}$)	η_{PDP} (%)
BDIQ	303	425.3	118.3	111.0	64.3	89.3
	313	435.5	285	106	62.6	80.7
	323	413.8	555	131	36	75.3
	333	435.6	1376	152	56.1	65.1
HDIQ	303	468.2	79.1	86.0	76.5	92.8
	313	431.5	186.4	101	57.0	87.3
	323	449.5	556.4	78.7	155.0	75.3
	333	442.3	1236	88.6	89.3	66.6

The activation indices such as the enthalpy (ΔH_a), activation energy (E_a), and entropy (ΔS_a) of activation were determined by the Arrhenius equation and its alternate form [51].

$$i_{corr} = k \exp\left(-\frac{E_a}{RT}\right) \tag{14}$$

$$i_{corr} = \frac{RT}{Nh} \exp\left(\frac{\Delta S_a}{R}\right) \exp\left(\frac{\Delta H_a}{RT}\right) \tag{15}$$

In the above equations (14 and 15), A denotes the pre-exponential Arrhenius constant, h refers to the constant of Planck, N refers to the Avogadro number, and R refers to the constant of the ideal gas.

The E_a values for in the inhibited medium and its non-inhibited counterpart were determined *via* the linear fit of $\ln i_{corr}$ *vs.* $\frac{1000}{T}$ plots (Figure 6).

The ΔH_a and ΔS_a values were determined by the slope and intercept of straight lines obtained from the $\ln\left(\frac{i_{corr}}{T}\right)$ *vs.* $\frac{1000}{T}$ (Figure 7) and tabulating them in Table 7.

Based on the findings in Table 6, the addition of BDIQ and HDIQ led to an increase in the E_a compared to the non-inhibited medium. This increase is due to the physical adsorption of these derivatives on CS and also reveals that more energy barriers are required for CS corrosion in their absence [52]. The positive value of ΔH_a reflects the endothermic character of the CS dissolution process and points out that CS dissolution is difficult in an uninhibited medium, implying that the metal's dissolution character is low. Furthermore, when BDIQ and HDIQ were present, the value of ΔS_a was raised, meaning that it was a rate-determining step [53]. The adsorption of such organic molecules on metallic surfaces is often greater than the desorption rate of water molecules in an acidic medium, which reflects the quasi-substitution process of the inhibitor molecule in CS/1 M HCl. The rising levels of ΔS_a can also be attributed to an increase in solvent entropy [54].

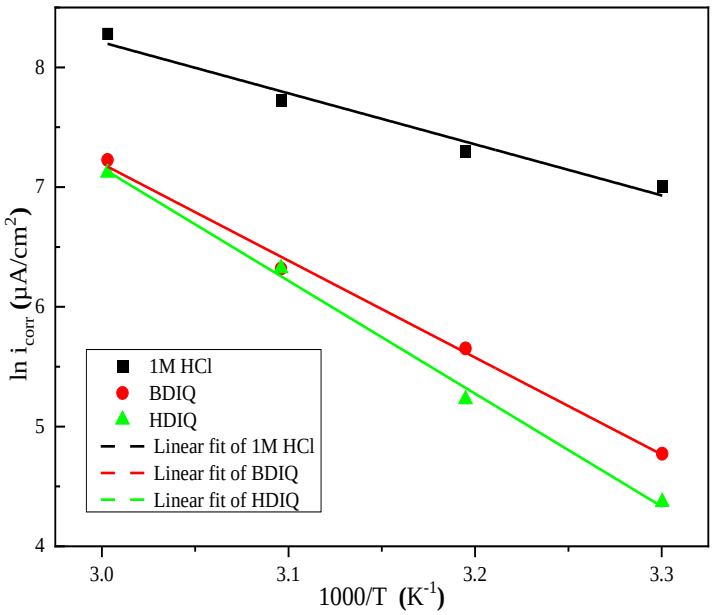

Figure 6. Arrhenius plots for CS dissolution in the inhibited medium and its non-inhibited counterpart at divers' temperatures.

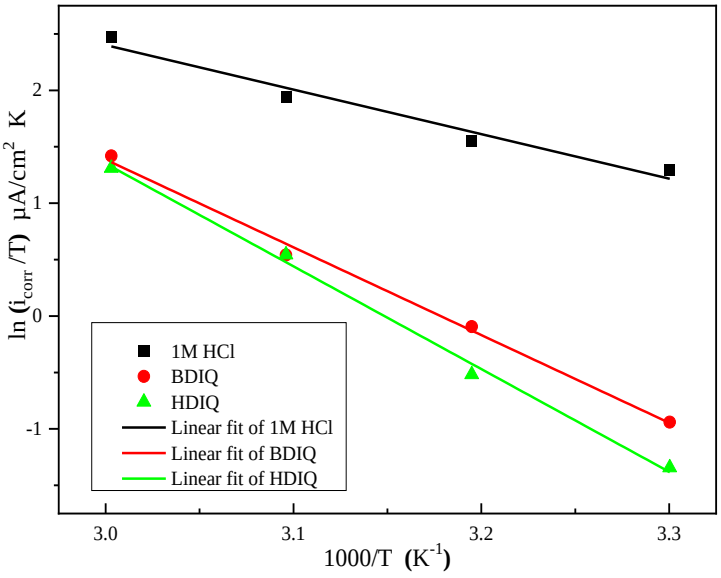

Figure 7. Alternative Arrhenius plots for CS dissolution in the inhibited medium and its non-inhibited counterpart at divers' temperatures.

Table 7. The activation indices for CS dissolution in the inhibited medium and its non-inhibited counterpart at diverse temperatures.

Medium	E_a **(kJ·mol^{-1})**	ΔH_a **(kJ·mol^{-1})**	ΔS_a **(J·mol^{-1}·K^{-1})**
Blank	35.4	32.76	–79.18
HDIQ	78.28	75.66	40.76
BDIQ	67.25	64.61	7.93

3.6. SEM-EDS analysis

Figure 8 shows SEM-EDS images of the CS surface before and after 24 h of dipping in 1 M HCl without and with 10^{-3} M of BDIQ and HDIQ at 303 K. The CS metal, before soaking, shows a clean surface with some distinctive lines that resulted from the abrasive machining (Figure 8(A)). Moreover, as noticed in Figure 8(B), the CS in the non-inhibited medium is severely damaged, and numerous pits appear covered with many corrosion products. After the addition of BDIQ and HDIQ (Figure 8 (D and C)), the enhanced and sparsely damaged surface of CS encourages the production of a protective layer, which stops corrosion. Whereas, Figure 8 reveals the EDS spectra of CS under multiple circumstances. The EDS spectrum depicted in Figure 8(A) emphasizes the distinctive peaks of the CS composition consisting of Fe, O, and C. However, after soaking CS in an acidic medium, the EDS spectrum in Figure 8(B) exhibits additional distinctive peaks of Cl, which reflect the HCl medium and Fe oxide elements, respectively. These peaks imply that corrosion products accumulated on the CS surface. H8owever, the peaks associated with the products of corrosion decreased, and the Cl peak disappeared when HDIQ and BDIQ were present, as portrayed in Figures 8(C, D).

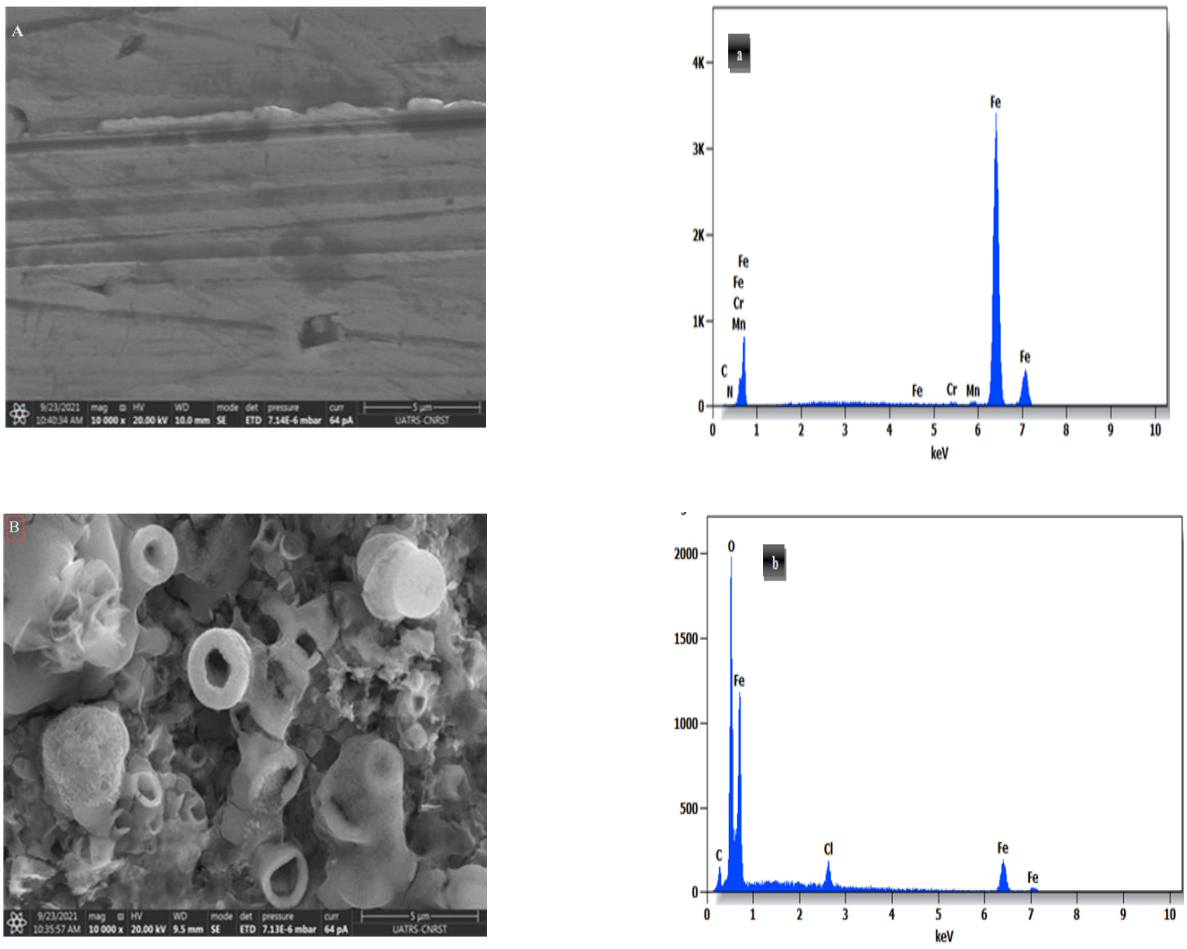

Figure 8. SEM-EDS images for CS surface under various conditions: before (A) and after immersion for 24 hours in 1 M HCl (B).

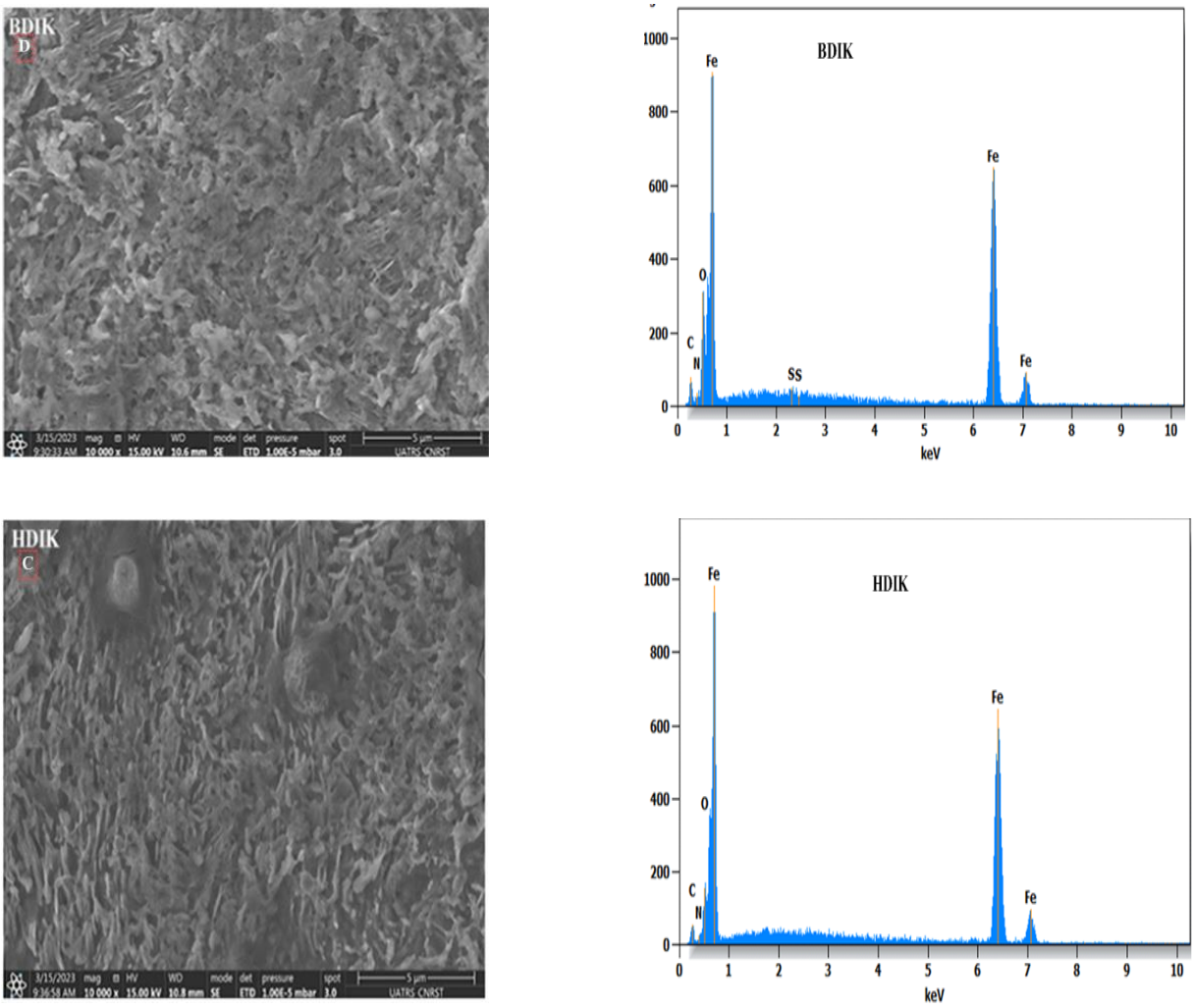

Figure 8. SEM-EDS images for CS surface under various conditions: after immersion for 24 hours in 1 M HCl+10^{-3} M of BDIQ (D), 1 M HCl+10^{-3} M of HDIQ (C).

3.7. DFT reactivity

To investigate the effectiveness of corrosion inhibition and evoke a plausible corrosion inhibition mechanism, the electronic properties, global activity descriptors, and local activity indices of HDIQ and BDIQ were calculated [55]. To maintain structural conformity, the absence of imaginary frequencies must be ascertained using the same level of theory. To plot the structure, HOMO, and LUMO of the compounds, Gauss View/5 software was applied.

Figure 9 depicts the energy-minimized structures and FMOs (HOMO and LUMO) of the HDIQ and BDIQ. The electronic representations of HOMO and LUMO show that these molecules have an almost total occupation, implying that the reactivity is very high with other species and especially with the metal surface.

Key	Optimized molecule	HOMO	LUMO
HDIQ	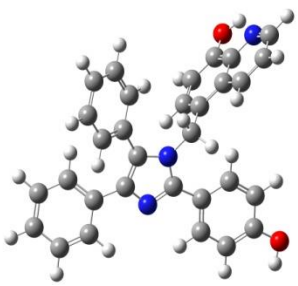	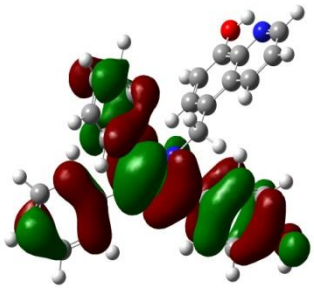	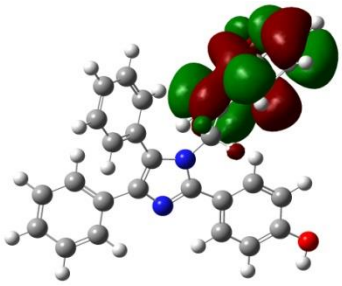
BDIQ	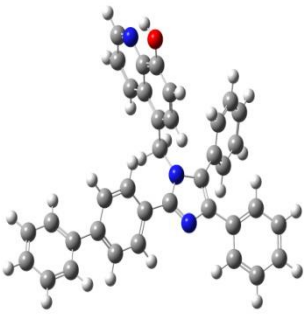	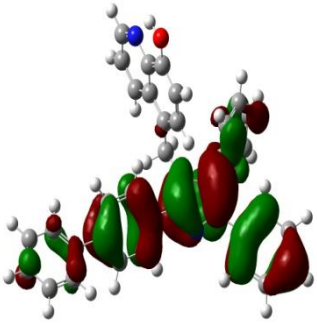	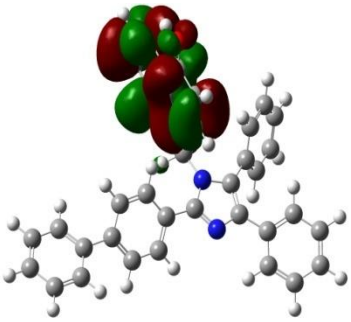

Figure 9. Optimized molecules and FMOs for HDIQ and BDIQ.

E_{HOMO} and E_{LUMO} values serve to assess the donor/acceptor ratio in the molecule/metal relationship [56]. In this study of quantum computation, the behaviour of the reactivity of the HDIQ and BDIQ is followed by these two descriptors. Table 8 groups the different values of the reactivity descriptors of both molecules.

The data in the Table 8 reveals that the HDIQ is more nucleophilic (E_{HOMO}=−4.993 eV) and the BDIQ is more electrophilic (E_{LUMO}=−1.782 eV). Therefore, ΔE (E_{LUMO}−E_{HOMO}) provides the latitude to judge a molecule's reactivity capacity, given that with the lowest value of this parameter, the reactivity of this molecule is maximal. The description comparison between both values of this descriptor (ΔE) shows that the HDIQ is more reactive with a low value of 3.239 eV, this is very agreeing with the experimental findings.

The electronegativity (χ) presents an attractive power of the electrons of a chemical species; the relevance of the descriptor translates the reactivity of interaction [57]. The value of 3.373 eV of HDIQ posted in Table 8 shows that this more reactive inhibitor. The reactivity and hardness (η) of a molecule are reciprocally proportional: a harder molecule implies lower reactivity. The data in Table 8 show that HDIQ is more reactive.

The values of ΔN_{110} provide important data on the tendency of the electrons to flow from the molecule to the CS surface (ΔN>0) or *vice versa* (ΔN<0) [58]. In this present computation, the HDIQ molecule (ΔN_{110}=0.447) is more likely to share its electron in order to form coordination bonds with Fe (110).

Table 8. Descriptors for reactivity of the HDIQ and BDIQ.

Key	E_{HOMO} (eV)	E_{LUMO} (eV)	ΔE (eV)	χ (eV)	η (eV)	ΔN_{110}
HDIQ	–4.993	–1.754	3.239	3.373	1.619	0.447
BDIQ	–5.170	–1.782	3.388	3.476	1.694	0.397

The inhibitory efficacy of a molecule can be measured and assessed by the prevalence of active sites throughout its structure. In addition, the sites of high local reactivity support substantial inhibitory efficacy. These centers may bind with others located on the metal surface by chemical bonds [59]. In Tables 9 and 10, the various sites of HDIQ and BDIQ are collected, respectively, with the most suitable atoms presenting the highest reactivity, giving the acceptor (nucleophilic attack ($f(+)$) and donor (electrophilic- attack ($f(-)$). The condensed Fukui functions ($f(+)$ and $f(-)$) for HDIQ and BDIQ indicated that C_{13}, C_{15}, and C_{16} are the most electrophilic attacks centers, whereas the atoms N_1, C_2, C_3, C_4, C_7, C_8, and C_9 are highest nucleophilic attacks centers.

Table 9. Atoms of local reactivity for HDIQ.

Atoms	$f(-)$	$f(+)$	Structure of HDIQ
N (1)	0.003	0.110	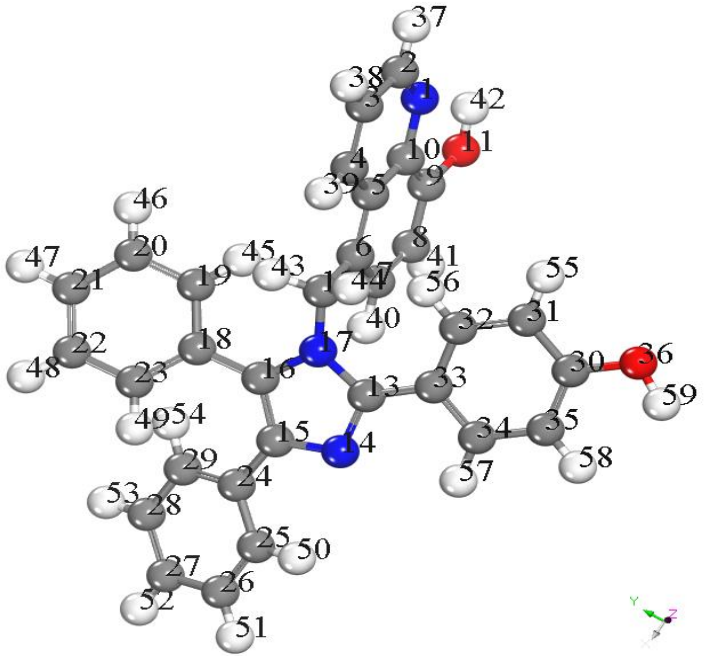
C (2)	0.003	0.093	
C (3)	0.003	0.075	
C (4)	0.001	0.109	
C (5)	0.001	0.029	
C (6)	0.005	0.041	
C (7)	0.000	0.052	
C (8)	0.003	0.061	
C (9)	0.005	0.058	
C (10)	0.003	0.041	
O (11)	0.004	0.044	
C (12)	0.005	0.006	
C (13)	0.050	0.001	
N (14)	0.042	0.006	
C (15)	0.057	0.004	
C (16)	0.063	0.000	
N (17)	0.016	0.004	
C (18)	0.021	0.001	
C (19)	0.030	0.000	
C (20)	0.027	0.003	
C (21)	0.043	0.003	
C (22)	0.024	0.003	

Atoms	*f* (–)	*f* (+)	Structure of HDIQ
C (23)	0.029	0.002	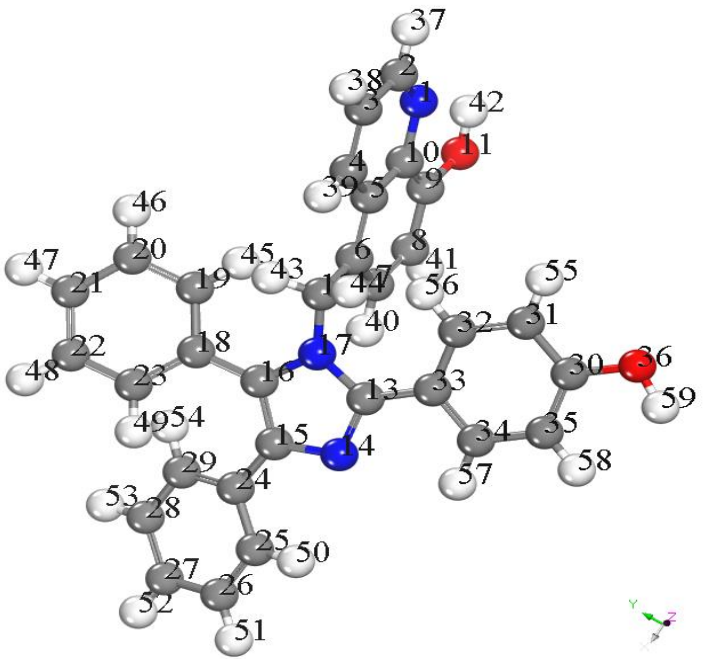
C (24)	0.019	0.000	
C (25)	0.030	0.002	
C (26)	0.025	0.002	
C (27)	0.038	0.002	
C (28)	0.022	0.001	
C (29)	0.026	0.001	
C (30)	0.034	0.003	
C (31)	0.025	0.004	
C (32)	0.028	0.001	
C (33)	0.022	0.001	
C (34)	0.031	0.003	
C (35)	0.024	0.004	
O (36)	0.032	0.002	

Table 10. A to CS of local reactivity for BDIQ.

Atoms	*f* (–)	*f* (+)	Structure of BDIQ
N (1)	0.003	0.110	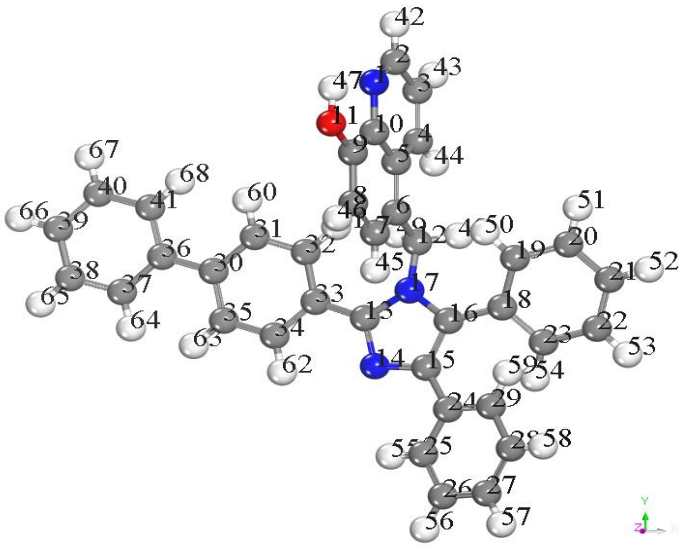
C (2)	0.003	0.093	
C (3)	0.003	0.074	
C (4)	0.001	0.109	
C (5)	0.001	0.029	
C (6)	0.005	0.042	
C (7)	0.000	0.052	
C (8)	0.003	0.061	
C (9)	0.004	0.058	
C (10)	0.002	0.041	
O (11)	0.004	0.044	
C (12)	0.004	0.006	
C (13)	0.046	0.001	
N (14)	0.037	0.006	
C (15)	0.052	0.004	
C (16)	0.058	0.000	
N (17)	0.015	0.004	

Atoms	*f* (–)	*f* (+)	Structure of BDIQ
C (18)	0.020	0.001	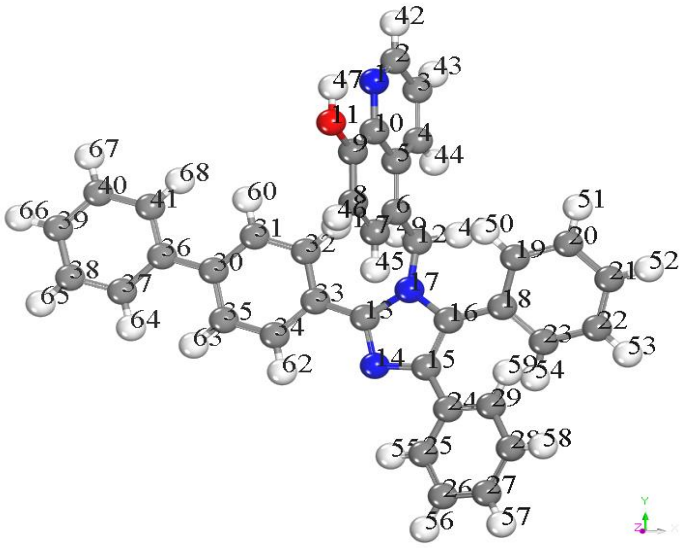
C (19)	0.028	0.000	
C (20)	0.026	0.003	
C (21)	0.041	0.003	
C (22)	0.023	0.003	
C (23)	0.027	0.002	
C (24)	0.017	0.000	
C (25)	0.027	0.002	
C (26)	0.023	0.001	
C (27)	0.035	0.002	
C (28)	0.020	0.001	
C (29)	0.023	0.001	
C (30)	0.032	0.003	
C (31)	0.021	0.003	
C (32)	0.026	0.001	
C (33)	0.019	0.000	
C (34)	0.028	0.003	
C (35)	0.020	0.003	
C (36)	0.010	0.000	
C (37)	0.017	0.001	
C (38)	0.012	0.001	
C (39)	0.022	0.002	
C (40)	0.012	0.001	
C (41)	0.017	0.001	

3.8. MD simulation

The MD method is often used as a simulation approach to assess inter- and intra-molecular interactions [60]. In this session of the work, this simulation deals with the reactivity of quinoline molecules and Fe (110). This research also investigated the influence of two attached motifs with the two molecules HDIQ and BDIQ on the effectiveness of surface protection against attack by corrosive species contained in the molar HCl solution. Figure 10 illustrates the adsorption of the species of interest (lateral representation) on Fe (110). Further analysis of these configurations reveals that both molecules adsorb wholly and largely occupy the iron atomic layer, resulting in a high percentage of anticorrosive protection.

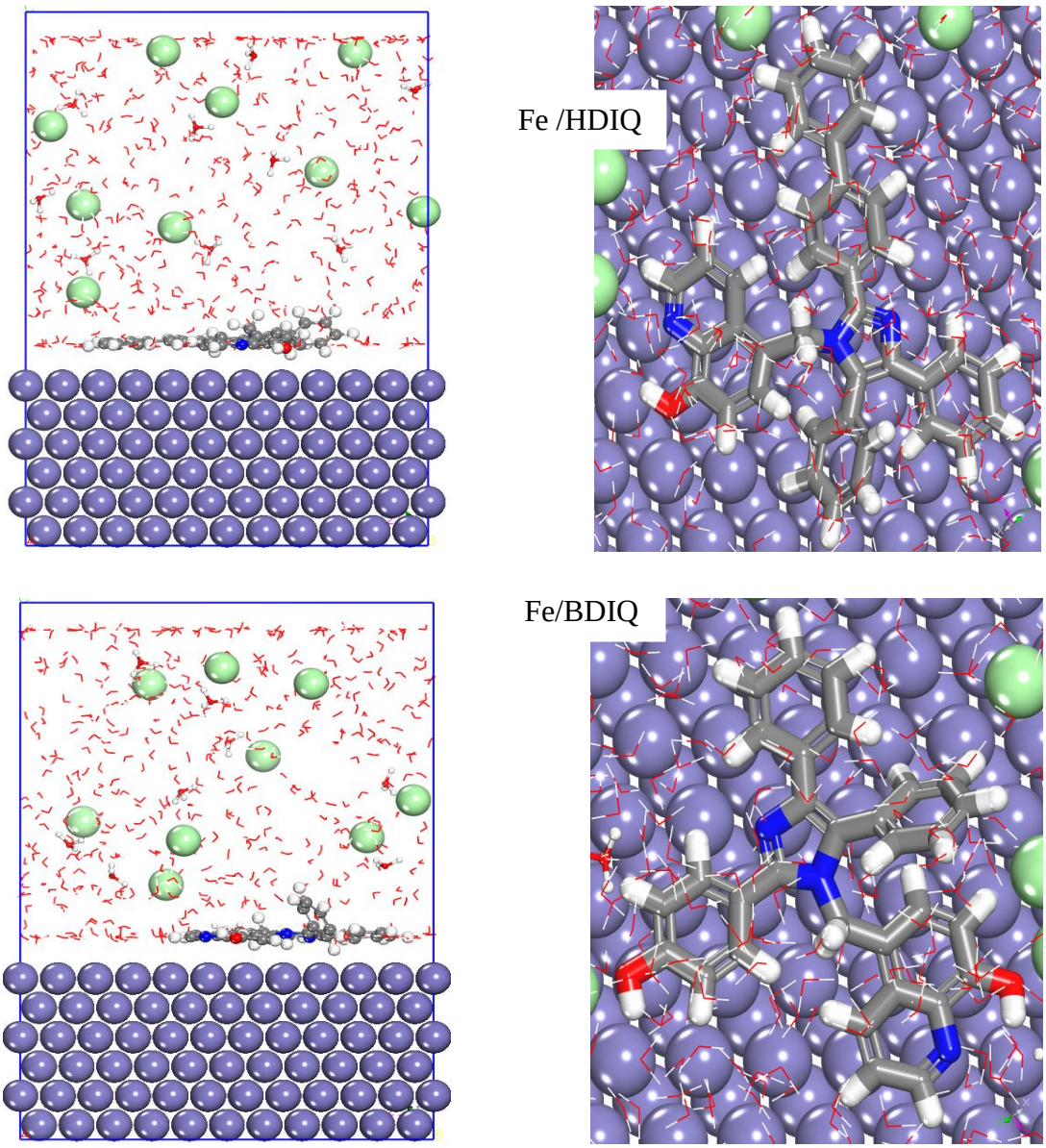

Figure 10. Absorption configurations of Fe/HDIQ and Fe/BDIQ.

The $E_{\text{interaction}}$ (E_{inter}) value is defined by the equation hereunder [61]:

$$E_{\text{inter}} = E_{(\text{surface+solution})} - E_{\text{inhibitor}} + E_{\text{total}^\circ} \quad (16)$$

The low value of E_{inter} attests to the interactions for Fe/HDIQ and Fe/BDIQ [62]. The values of this descriptor for both systems are calculated and listed in Table 11, it appears from the comparative study that the most negative value of Fe/HDIQ (–941.049 kJ·mol^{-1}) reflects a larger interaction. These simulation data clearly prove the agreement compared with the experimental study and the quantum computations.

Table 11. E_{inter} for both systems Fe/HDIQ and Fe/BDIQ.

Systems	Fe/HDIQ	Fe/BDIQ
E_{inter} (kJ·mol^{-1})	–941.049	–923.597

In order to better perceive the nature of the bonds occurring between the studied inhibitor and the Fe atoms, the radial distribution function (RDF) method is applied. The latter is a valuable tool for the determination of the interatomic distances for inhibitor/Fe [63]. The published literature confirmed that the likelihood of chemical adsorption was higher when the bond length was less than 3.5 Å. By contrast, physical adsorption is more probable [64]. In Figure 11, the spectral data from this method are illustrated. The first peaks reveal the chemical bond length values for both for CS.

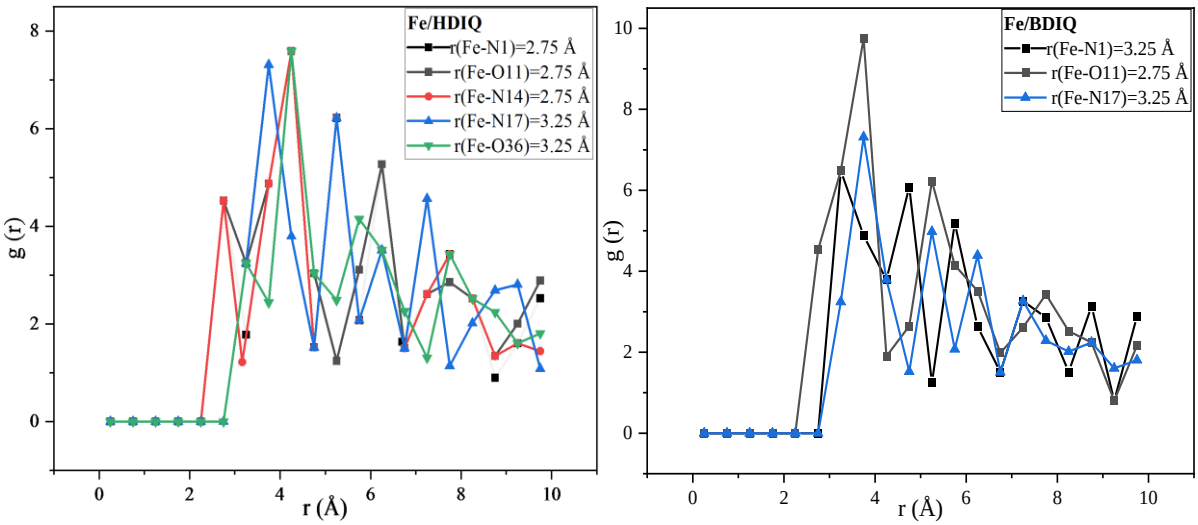

Figure 11. RDF of Fe/HDIQ and Fe/BDIQ.

Conclusion

The current study deals with the examination of two heterocyclic molecules, namely 5-((2-(4-hydroxyphenyl)-4,5-diphenyl-1*H*-imidazol-1-yl)methyl)quinolin-8-ol (HDIQ) and 5-((2-([1,1′-biphenyl]-4-yl)-4,5-diphenyl-1*H*-imidazol-1-yl)methyl)quinolin-8-ol (BDIQ) for carbon steel corrosion inhibition in 1 M HCl. Approaches such as weight loss, electrochemical, computational, and surface (SEM-EDS) analysis were conducted to assess the anticorrosion performance of HDIQ and BDIQ. The succeeding conclusions were reached:

- The PDP measurements demonstrated that the anti-corrosion potency of HDIQ and BDIQ is concentration- and temperature-dependent.
- 8-Hydroxyquinoline-imidazole derivatives were chemisorbed onto CS in a 1 M HCl solution according to the Langmuir isotherm.

- According to PDP data, the 8-hydroxyquinoline-imidazole derivatives act as mixed-type inhibitors;
- SEM-EDS data suggest the presence of a thin protective film of 8-hydroxyquinoline-imidazole molecules on the metal surface.
- Data collected in theoretical approaches confirm the findings of the experiment.

References

1. H. Zheng, B. Zhang, X. Wang, Y. Lu, F. Li and C. Li, Improved corrosion resistance of carbon steel in soft water with dendritic-polymer corrosion inhibitors, *Chem. Eng. J*., 2023, **452**, 139043. doi: 10.1016/j.cej.2022.139043
2. J. Lazrak, E. Ech-chihbi, B. El Ibrahimi, F. El Hajjaji, Z. Rais, M. Tachihante and M. Taleb, Detailed DFT/MD simulation , surface analysis and electrochemical computer explorations of aldehyde derivatives for mild steel in 1.0 M HCl, *Colloids Surf., A*, 2022, **632**, 127822. doi: 10.1016/j.colsurfa.2021.127822
3. S. Sengupta, M. Murmu, N.C. Murmu and P. Banerjee, Adsorption of redox-active Schiff bases and corrosion inhibiting property for mild steel in 1 $molL^{-1}$ H_2SO_4: Experimental analysis supported by *ab initio* DFT, DFTB and molecular dynamics simulation approach, *J. Mol. Liq*., 2021, **326**, 115215. doi: 10.1016/j.molliq.2020.115215
4. D.B. Tripathy, M. Murmu, P. Banerjee and M.A. Quraishi, Palmitic acid based environmentally benign corrosion inhibiting formulation useful during acid cleansing process in MSF desalination plants, *Desalination*, 2019, **472**, 114128. doi: 10.1016/j.desal.2019.114128
5. A. Zarrouk, H. Zarrok, R. Salghi, R. Touir, B. Hammouti, N. Benchat, L.L. Afrine, H. Hannache, M. El Hezzat and M. Bouachrine, Electrochemical impedance spectroscopy weight loss and quantum chemical study of new pyridazine derivative as inhibitor corrosion of copper in nitric acid, *J. Chem. Pharm. Res*., 2013, **5**, no. 12, 1482–1491.
6. A. Zarrouk, H. Zarrok, R. Salghi, N. Bouroumane, B. Hammouti, S.S. Al-Deyab and R. Touzani, The Adsorption and Corrosion Inhibition of 2-[Bis-(3,5-dimethyl-pyrazol-1-ylmethyl)-amino]-pentanedioic Acid on Carbon Steel Corrosion in 1.0 m HCl, *Int. J. Electrochem. Sci*., 2012, **7**, 10215–10232.
7. H. Bendaha, A. Zarrouk, A. Aouniti, B. Hammouti, S. El Kadiri, R. Salghi and R. Touzani, Adsorption and corrosion inhibitive properties of some tripodal pyrazolic compounds on mild steel in hydrochloric acid systems, *Phys. Chem. News*, 2012, **64**, 95–103.
8. A. Zarrouk, B. Hammouti, H. Zarrok, I. Warad and M. Bouachrine, N-containing organic compound As An Effective Corrosion Inhibitor For Copper In 2 M HNO_3: Weight Loss and Quantum Chemical Study, *Der Pharm. Chem*., 2011, **3**, no. 5, 263–271.

9. H. Zarrok, R. Saddik, H. Oudda, B. Hammouti, A. El Midaoui, A. Zarrouk, N. Benchata and M. Ebn Touhami, 5-(2-chlorobenzyl)-2,6-dimethylpyridazin-3-one: An efficient inhibitor of C38 steel corrosion in hydrochloric acid, *Der Pharm. Chem*., 2011, **3**, no. 5, 272–282.
10. A. Zarrouk, B. Hammouti, R. Touzani, S.S. Al-Deyab, M. Zertoubi, A. Dafali and S. Elkadiri, Comparative study of new quinoxaline derivatives towards corrosion of copper in nitric acid, *Int. J. Electrochem. Sci*., 2011, **6**, 4939–4952.
11. V. Saraswat, R. Kumaria and M. Yadav, Novel carbon dots as efficient green corrosion inhibitor for mild steel in HCl solution : Electrochemical, gravimetric and XPS studies, *J. Phys. Chem. Solids*., 2022, **160**, 110341. doi: 10.1016/j.jpcs.2021.110341
12. Y. Morozov, L.M. Calado, R.A. Shakoor, R. Raj, R. Kahraman, M.G. Taryba and M.F. Montemor, Epoxy coatings modified with a new cerium phosphate inhibitor for smart corrosion protection of steel, *Corros. Sci*., 2019, **159**, 108128. doi: 10.1016/j.corsci.2019.108128
13. C. Verma, M.A. Quraishi and E.E. Ebenso Quinoline and its derivatives as corrosion inhibitors: A review, *Surf. Interfaces*, 2020, **21**, 100634. doi: 10.1016/j.surfin.2020.100634
14. Z.M. Alamshany and A.A. Ganash, Synthesis, characterization, and anti-corrosion properties of an 8-hydroxyquinoline derivative, *Heliyon*, 2019, **5**, no. 11, e02895. doi: 10.1016/J.HELIYON.2019.E02895
15. G.P. Cicileo, B.M. Rosales, F.E. Varela and J.R. Vilche, Inhibitory action of 8-HYDROXYQUINOLINE on the copper corrosion process, *Corros. Sci*., 1998, **40**, no. 11, 1915–1926. https://doi.org/10.1016/S0010-938X(98)00090-0
16. E. Berdimurodov, C. Verma, K. Berdimuradov, M.A. Quraishi, A. Kholikov, K. Akbarov, N. Umirov and B. Borikhonov, 8-Hydroxyquinoline is key to the development of corrosion inhibitors: An advanced review, *Inorg. Chem. Commun*., 2022, **144**, 109839. doi 10.1016/j.inoche.2022.109839
17. J. You and Z. Liu, Atomistic simulation of corrosion protection of Al_2Cu aluminum alloy by 8-hydroxyquinoline, *Appl. Surf. Sci*., 2021, **540**, 148315. doi: 10.1016/j.apsusc.2020.148315
18. M. El Faydy, B. Lakhrissi, C. Jama, A. Zarrouk, L.O. Olasunkanmi, E.E. Ebenso and F. Bentiss, Electrochemical, surface and computational studies on the inhibition performance of some newly synthesized 8-hydroxyquinoline derivatives containing benzimidazole moiety against the corrosion of carbon steel in phosphoric acid environment, *J. Mater. Res. Technol*., 2020, **9**, no. 1, 727–748. doi: 10.1016/j.jmrt.2019.11.014
19. Y. Song, H. Xu, W. Chen, P. Zhan and X. Liu, 8-Hydroxyquinoline: a privileged structure with a broad-ranging pharmacological potential, *Med. Chem. Comm*., 2015, **6**, no. 1, 61–74. doi: 10.1039/C4MD00284A
20. V. Oliveri and G. Vecchio, 8-Hydroxyquinolines in medicinal chemistry: A structural perspective, *Eur. J. Med. Chem*., 2016, **120**, 252–274. doi: 10.1016/j.ejmech.2016.05.007

21. Standard Practice for Preparing, Cleaning, and Evaluating Corrosion Test Specimens. Designation: G1-03, *ASTM Spec. Tech. Publ*., 2017, 505–510.
22. V. Saraswat and M. Yadav, Computational and electrochemical analysis on quinoxalines as corrosion inhibitors for mild steel in acidic medium, *J. Mol. Liq*., 2020, **297**, 111883. doi: 10.1016/j.molliq.2019.111883
23. G. Laadam, F. Benhiba, M. El Faydy, A. Titi, A.S. Al-Gorair, M. Alshareef, H. Hawsawi, R. Touzani, I. Warad, A. Bellaouchou, A. Guenbour, M. Abdallah and A. Zarrouk, Anti-corrosion performance of novel pyrazole derivative for carbon steel corrosion in 1 M HCl: Computational and experimental studies, *Inorg. Chem. Commun*., 2022, **145**, 109963. doi: 10.1016/j.inoche.2022.109963
24. W. Al Garadi, K. Jrajri, M. El Faydy, F. Benhiba, L. El Ghayati, N.K. Sebbar, E.M. Essassi, I. Warad, A. Guenbour, A. Bellaouchou, C. Jama, A. Alsalme and A. Zarrouk, 4-phenyl-decahydro-1*H*-1,5-benzodiazepin-2-one as novel and effective corrosion inhibitor for carbon steel in 1 M HCl solution: A combined experimental and empirical studies, *J. Indian Chem. Soc*., 2022, **99**, no. 11, 100742. doi: 10.1016/j.jics.2022.100742
25. A. Fatah, N. Timoudan, M. Rbaa, F. Benhiba, R. Hsissou, Z.S. Safi, I. Warad, A.A. Al Obaid, B.M. Al-Maswari, A. Boutakiout, H. Zarrok, B. Lakhrissi, A. Bellaouchou, C. Jama, F. Bentiss, H. Oudda and A. Zarrouk, Assessment of New Imidazol Derivatives and Investigation of Their Corrosion-Reducing Characteristics for Carbon Steel in HCl Acid Solution, *Coatings*, 2023, **13**, 8, 1405. doi: 10.3390/coatings13081405
26. V. Saraswat and M. Yadav, Computational and electrochemical analysis on quinoxalines as corrosion inhibitors for mild steel in acidic medium, *J. Mol. Liq*., 2020, **297**, 111883. doi: 10.1016/j.molliq.2019.111883
27. I.B. Onyeachu, I.B. Obot, A.A. Sorour and M.I. Abdul-Rashid, Green corrosion inhibitor for oilfield application I: Electrochemical assessment of 2-(2-pyridyl) benzimidazole for API X60 steel under sweet environment in NACE brine ID196, *Corros. Sci*., 2019, **150**, 183–193. doi: 10.1016/j.corsci.2019.02.010
28. J. Saranya, F. Benhiba, N. Anusuya, R. Subbiah, A. Zarrouk and S. Chitra, Experimental and computational approaches on the pyran derivatives for acid corrosion, *Colloids Surf. A*, 2020, **603**, 125231. doi: 10.1016/j.colsurfa.2020.125231
29. R. Hsissou, F. Benhiba, M. Khudhair, M. Berradi, A. Mahsoune, H. Oudda, A. El Harfi, I.B. Obot and A. Zarrouk, Investigation and comparative study of the quantum molecular descriptors derived from the theoretical modeling and Monte Carlo simulation of two new macromolecular polyepoxide architectures TGEEBA and HGEMDA, *Journal of King Saud University – Science*, 2020, **32**, no. 1, 667–676. doi: 10.1016/j.jksus.2018.10.008
30. M. El Faydy, M. Rbaa, L. Lakhrissi, B. Lakhrissi, I. Warad, A. Zarrouk and I.B. Obot, Corrosion protection of carbon steel by two newly synthesized benzimidazol-2-ones substituted 8-hydroxyquinoline derivatives in 1 M HCl: Experimental and theoretical study, *Surf. Interfaces*, 2019, **14**, 222–237. doi: 10.1016/j.surfin.2019.01.005

31. M.J. Frisch, G.W. Trucks, H.B. Schlegel, G.E. Scuseria, M.A. Robb, J.R. Cheeseman, G. Scalmani, V. Barone, B. Mennucci, G.A. Petersson, H. Nakatsuji, M. Caricato, X. Li, H.P. Hratchian, A.F. Izmaylov, J. Bloino, G. Zheng, J.L. Sonnenberg, M. Hada, M. Ehara, K. Toyota, R. Fukuda, J. Hasegawa, M. Ishida, T. Nakajima, Y. Honda, O. Kitao, H. Nakai, T. Vreven, J.A. Montgomery, Jr., J.E. Peralta, F. Ogliaro, M. Bearpark, J.J. Heyd, E. Brothers, K.N. Kudin, V.N. Staroverov, R. Kobayashi, J. Normand, K. Raghavachari, A. Rendell, J.C. Burant, S.S. Iyengar, J. Tomasi, M. Cossi, N. Rega, J.M. Millam, M. Klene, J.E. Knox, J.B. Cross, V. Bakken, C. Adamo, J. Jaramillo, R. Gomperts, R.E. Stratmann, O. Yazyev, A.J. Austin, R. Cammi, C. Pomelli, J.W. Ochterski, R.L. Martin, K. Morokuma, V.G. Zakrzewski, G.A. Voth, P. Salvador, J.J. Dannenberg, S. Dapprich, A.D. Daniels, Ö. Farkas, J.B. Foresman, J.V. Ortiz, J. Cioslowski and D.J. Fox, *Gaussian 09, Revision C.01*, Gaussian, Inc., Wallingford CT, 2009.
32. Y. Boughoues, M. Benamira, L. Messaadia, N. Bouider and S. Abdelaziz, Experimental and theoretical investigations of four amine derivatives as effective corrosion inhibitors for mild steel in HCl medium, *RSC Adv*., 2020, **10**, no. 40, 24145–24158. doi: 10.1039/D0RA03560B
33. W.K. Al-Azzawi, A.J. Al Adily, F.F. Sayyid, R.K. Al-Azzawi, M.H. Kzar, H.N. Jawoosh, A.A. Al-Amiery, A.A.H. Kadhum, W.N.R.W. Isahak and M.S. Takriff, Evaluation of corrosion inhibition characteristics of an *N*-propionanilide derivative for mild steel in 1 M HCl: Gravimetrical and computational studies, *Int. J. Corros. Scale Inhib*., 2022, **11**, no. 3, 1100–1114. doi: 10.17675/2305-6894-2022-11-3-12
34. T. Raja, S.S. Syed Abuthahir, A. Samsath Begum, M. Lavanya and S. Rajendran, Corrosion inhibition performance of carbon steel in 1 N hydrochloric acid by an aqueous extract of *Syzygium cumini Linn* (SCL) plant leaves, *Int. J. Corros. Scale Inhib*., 2022, **11**, no. 4, 1819–1838. doi: 10.17675/2305-6894-2022-11-4-26
35. M.D. Plotnikova, A.D. Shitoeva, A.D. Solovyev, A.N. Bakiev and A.B. Shein, Some aspects of the of the mechanism of C1018 steel protection in hydrochloric acid solutions by triazole derivatives, *Int. J. Corros. Scale Inhib*., 2023, **12**, no. 2, 511–530. doi 10.17675/2305-6894-2023-12-2-8
36. W.N. Ahmaeed, A.N. Abd and A.A. Khadom, Corrosion inhibition effect of sodium iodide for mild steel in 1 M hydrochloric acid: Gravimetrical and electrochemical studies, *Int. J. Corros. Scale Inhib*., 2019, **8**, no. 4, 1097–1111. doi: 10.17675/2305-6894-2019-8-4-17
37. A.G. Berezhnaya, V.V. Chernyavina and L.M. Astakhova, Imidazobenzimidazole hydrochloride derivatives as steel inhibitors in hydrochloric acid, *Int. J. Corros. Scale Inhib*., 2020, **9**, no. 1, 313–319. doi: 10.17675/2305-6894-2020-9-1-20

38. L.E. Tsygankova, A.E. Abramov, A.A. Uryadnikov, T.V. Semenyuk, K.O. Strel'nikova, R.K. Vagapova and O.G. Mikhalkina, Study of the protection of carbon steel with an inhibitory composition in hydrogen sulfide environments by electrochemical methods, *Int. J. Corros. Scale Inhib*., 2023, **12**, no. 3, 811–824. doi: 10.17675/2305-6894-2023-12-3-1
39. H. Zarrok, A. Zarrouk, R. Salghi, H. Oudda, B. Hammouti, M. Ebn Touhami, M. Bouachrine and O.H. Pucci, A Combined Experimental and Theoretical Study on the Corrosion Inhibition and Adsorption Behaviour of Quinoxaline Derivative During Carbon Steel Corrosion in Hydrochloric Acid, *Port. Electrochim. Acta*, 2012, **30**, no. 6, 405–417. doi: 10.4152/pea.201206405
40. M. Yadav, L. Gope, N. Kumari and P. Yadav, Corrosion inhibition performance of pyranopyrazole derivatives for mild steel in HCl solution: Gravimetric, electrochemical and DFT studies, *J. Mol. Liq*., 2016, **216**, 78–86. doi: 10.1016/j.molliq.2015.12.106
41. M. El Azzouzi, A. Aouniti, M. El Massaoudi, S. Radi, B. Hammouti, M.A. Quraishi, H. Bendaif and Y. El Ouadi, Inhibition effect of 1,1′-(pyridine-2,6-dihylbis(methylene))bis(5-methyl-1-*H*-pyrazole-3-carboxylic acid) on the corrosion of mild steel in 1 M HCl. Part A: Experimental study, *Int. J. Corros. Scale Inhib*., 2017, **6**, no. 4, 463–475, doi: 10.17675/2305-6894-2017-6-4-6
42. A. Molhi, R. Hsissou, M. Damej, A. Berisha, V. Thaçi, A. Belafhaili, M. Benmessaoud, N. Labjar and S. El Hajjaji, Contribution to the corrosion inhibition of C38 steel in 1 M hydrochloric acid medium by a new epoxy resin PGEPPP, *Int. J. Corros. Scale Inhib*., 2021, **10**, no. 1, 399–418. doi: 10.17675/2305-6894-2021-10-1-23
43. T. Raja, S.S. Syed Abuthahir, A. Samsath Begum, M. Lavanya and S. Rajendran, Corrosion inhibition performance of carbon steel in 1 N hydrochloric acid by an aqueous extract of *Syzygium cumini Linn* (SCL) plant leaves, *Int. J. Corros. Scale Inhib*., 2022, **11**, no. 4, 1819-1838, doi: 10.17675/2305-6894-2022-11-4-26
44. P. Singh, V. Srivastava and M.A. Quraishi, Novel quinoline derivatives as green corrosion inhibitors for mild steel in acidic medium: electrochemical, SEM, AFM, and XPS studies, *J. Mol. Liq*., 2016, **216**, 164–173. doi: 10.1016/j.molliq.2015.12.086
45. X. Li, S. Deng and H. Fu, Benzyltrimethylammonium iodide as a corrosion inhibitor for steel in phosphoric acid produced by dihydrate wet method process, *Corros.Sci*., 2011, **53**, no. 2, 664–670. doi: 10.1016/j.corsci.2010.10.013
46. R. Hsissou, O. Dagdag, S. Abbout, F. Benhiba, M. Berradi, M. El Bouchti, A. Berisha, N. Hajjaji and A. Elharfi, Novel derivative epoxy resin TGETET as a corrosion inhibition of E24 carbon steel in 1.0 M HCl solution. Experimental and computational (DFT and MD simulations) methods, *J. Mol. Liq*., 2019, **284**, 182–192. doi: 10.1016/j.molliq.2019.03.180
47. P. Singh, V. Srivastava and M.A. Quraishi, Novel quinoline derivatives as green corrosion inhibitors for mild steel in acidic medium: Electrochemical, SEM, AFM, and XPS studies, *J. Mol. Liq*., 2016, **216**, 164–173. doi: 10.1016/j.molliq.2015.12.086

48. I. Nadi, Z. Belattmania, B. Sabour, A. Reani, A. Sahibed-dine, C. Jama and F. Bentiss, *Sargassum muticum* extract based on alginate biopolymer as a new efficient biological corrosion inhibitor for carbon steel in hydrochloric acid pickling environment: Gravimetric, electrochemical and surface studies, *Int. J. Biol. Macromol*., 2019, **141**, 137–149. https://doi.org/10.1016/j.ijbiomac.2019.08.253
49. R.S. Abdel Hameed and A.H. Shamroukh, Synthesis, characterization, and evaluation of some acyclic *S*-nucleosides of pyrazolo[3,4-d]pyrimidine-thiones as corrosion inhibitors for carbon steel in hydrochloric acid, *Int. J. Corros. Scale Inhib*., 2017, **6**, no. 3, 333–348. doi: 10.17675/2305-6894-2017-6-3-8
50. T.K. Chaitra, K.N. Mohana, D.M. Gurudatt and H.C. Tandon, Inhibition activity of new thiazole hydrazones towards mild steel corrosion in acid media by thermodynamic, electrochemical and quantum chemical methods, *J. Taiwan Inst. Chem. Eng*., 2016, **67**, 521–531. doi: 10.1016/j.jtice.2016.08.013
51. S. El Arrouji, K. Karrouchi, I. Warad, A. Berisha, K.I. Alaoui, Z. Rais, S. Radi, M. Taleb, M. Ansar and A. Zarrouk, Multidimensional analysis for corrosion inhibition by new pyrazoles on mild steel in acidic environment: Experimental and computational approach, *Chem. Data Collect*., 2022, **40**, 100885. doi: 10.1016/J.CDC.2022.100885
52. P. Mourya, P. Singh, A.K. Tewari, R.B. Rastogi and M.M. Singh, Relationship between structure and inhibition behaviour of quinolinium salts for mild steel corrosion: Experimental and theoretical approach, *Corros. Sci*., 2015, **95**, 71–87. doi: 10.1016/j.corsci.2015.02.034
53. G.A. Zhang, X.M. Hou, B.S. Hou and H.F. Liu, Benzimidazole derivatives as novel inhibitors for the corrosion of mild steel in acidic solution: Experimental and theoretical studies, *J. Mol. Liq*., 2019, **278**, 413–427. doi: 10.1016/j.molliq.2019.01.060
54. M.A. Hegazy, R.M. Samy, A. Labena, M.A.M. Wadaan and W.N. Hozzein, 4,4′-(((1E,5E)-pentane-1,5-diylidene)bis(azanylylidene))bis(1-dodecylpyridin-1-ium)bromide as a novel corrosion inhibitor in an acidic solution (part I), *Mater. Sci. Eng. C*, 2020, **110**, 110673. doi: 10.1016/j.msec.2020.110673
55. M. Abdallah, H.M. Eltass, M.A. Hegazy and H. Ahmed, Adsorption and inhibition effect of novel cationic surfactant for pipelines carbon steel in acidic solution, *Prot. Met. Phys. Chem*., 2016, **52**, 721–730. doi: 10.1134/S207020511604002X
56. M. Bouklah, B. Hammouti, M. Lagrenée and F. Bentiss, Thermodynamic properties of 2,5-bis(4-methoxyphenyl)-1,3,4-oxadiazole as a corrosion inhibitor for mild steel in normal sulfuric acid medium, *Corros. Sci*., 2006, **48**, no. 9, 2831–2842. doi: 10.1016/j.corsci.2005.08.019
57. A. El yaktini, A. Lachiri, M. El Faydy, F. Benhiba, H. Zarrok, M. El Azzouzi, M. Zertoubi, M. Azzi, B. Lakhrissi and A. Zarrouk, Inhibitor effect of new azomethine derivative containing an 8-hydroxyquinoline moiety on corrosion behavior of mild carbon steel in acidic media, *Int. J. Corros. Scale Inhib*., 2018, **7**, no. 4, 609–632. doi: 10.17675/2305-6894-2018-7-4-9

58. F. Benhiba, N.K. Sebbar, H. Bourazmi, M.E. Belghiti, R. Hsissou, T. Hökelek, A. Bellaouchou, A. Guenbour, I. Warad, H. Oudda, A. Zarrouk and E.M. Essassi, Corrosion inhibition performance of 4-(prop-2-ynyl)-[1,4]-benzothiazin-3-one against CS in 1 M HCl solution: Experimental and theoretical studies, *Int. J. Hydrogen Energy*, 2022, **46**, no. 51, 25800–25818. doi: 10.1016/j.ijhydene.2021.05.091
59. R. Hamed, S. Jodeh, G. Hanbali, Z. Safi, A. Berisha, K. Xhaxhiu and O. Dagdag, Eco-friendly synthesis and characterization of double-crossed Link 3D graphene oxide functionalized with chitosan for adsorption of sulfamethazine from aqueous solution: Experimental and DFT calculations, *Front. Environ. Sci*., 2022, **10**, 930693. doi: 10.3389/fenvs.2022.930693
60. F. Benhiba, R. Hsissou, K. Abderrahim, H. Serrar, Z. Rouifi, S. Boukhris, G. Kaichouh, A. Bellaouchou, A. Guenbour, H. Oudda, I. Warad and A. Zarrouk, Development of new pyrimidine derivative inhibitor for mild steel corrosion in acid medium, *J. Bio-Tribo-Corros*., 2022, **8**, no. 2, 36. doi: 10.1007/s40735-022-00637-5
61. M. El Faydy, F. Benhiba, I. Warad, S. Saoiabi, A. Alharbi, A.A. Alluhaybi, B. Lakhrissi, M. Abdallah and A. Zarrouk, Bisquinoline analogs as corrosion inhibitors for carbon steel in acidic electrolyte: Experimental, DFT, and molecular dynamics simulation approaches, *J. Mol. Struct*., 2022, **1265**, 133389. doi: 10.1016/j.molstruc.2022.133389
62. M. Abouchane, N. Dkhireche, M. Rbaa, F. Benhiba, M. Ouakki, M. Galai, B. Lakhrissi, A. Zarrouk and M. Ebn Touhami, Insight into the corrosion inhibition performance of two quinoline-3-carboxylate derivatives as highly efficient inhibitors for CS in acidic medium: Experimental and theoretical evaluations, *J. Mol. Liq*., 2022, **360**, 119470. doi: 10.1016/j.molliq.2022.119470
63. D.K. Verma, S. Kaya, E. Ech-chihbi, F. El-Hajjaji, M.M. Phukan and H.M. Alnashiri, Investigations on some coumarin based corrosion inhibitors for mild steel in aqueous acidic medium: Electrochemical, surface morphological, density functional theory and Monte Carlo simulation approach, *J. Mol. Liq*., 2011, **329**, 115531. doi: 10.1016/j.molliq.2021.115531
64. B. El Ibrahimi, A. Jmiai, K. El Mouaden, R. Oukhrib, A. Soumoue, S. El Issami and L. Bazzi, Theoretical evaluation of some α-amino acids for corrosion inhibition of copper in acidic medium: DFT calculations, Monte Carlo simulations and QSPR studies, *J. King Saud Uni. – Sci*., 2020, **32**, no. 1, 163–171. doi: 10.1016/j.jksus.2018.04.004

♦ ♦ ♦